

ADAPT: Alzheimer’s Diagnosis through Adaptive Profiling Transformers

Yifeng Wang¹ Ke Chen¹ Haohan Wang¹

Abstract

Automated diagnosis of Alzheimer’s Disease (AD) from brain imaging, such as magnetic resonance imaging (MRI), has become increasingly important and has attracted the community to contribute many deep learning methods. However, many of these methods are facing a trade-off that 3D models tend to be complicated while 2D models cannot capture the full 3D intricacies from the data. In this paper, we introduce a new model structure for diagnosing AD, and it can complete with 3D model’s performances while essentially is a 2D method (thus computationally efficient). While the core idea lies in new perspective of cutting the 3D images into multiple 2D slices from three dimensions, we introduce multiple components that can further benefit the model in this new perspective, including adaptively selecting the number of slices in each dimension, and the new attention mechanism. In addition, we also introduce a morphology augmentation, which also barely introduces new computational loads, but can help improve the diagnosis performances due to its alignment to the pathology of AD. We name our method ADAPT, which stands for Alzheimer’s Diagnosis through Adaptive Profiling Transformers. We test our model from a practical perspective (the testing domains do not appear in the training one): the diagnosis accuracy favors our ADAPT, while ADAPT uses less parameters than most 3D models use.

1. Introduction

Alzheimer’s disease (AD) is a highly common neurodegenerative disorder that is usually diagnosed by structural alterations of the brain mass. Assessing an AD usually involves the acquisition of magnetic resonance imaging (MRI) images, since it offers accurate visualization of the anatomy and pathology of the brain (Zhou et al., 2023b). To over-

¹University of Illinois at Urbana-Champaign. Correspondence to: Haohan Wang <haohanw@illinois.edu>.

Preprint.

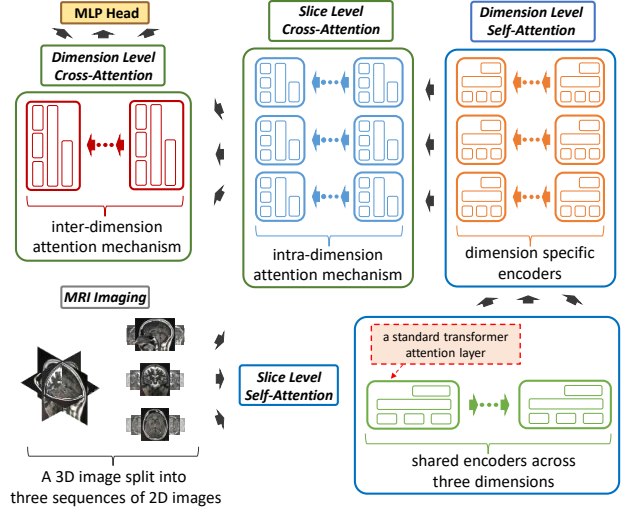


Figure 1. The overall framework of our proposed 2D ViT-Based Model for 3D Medical Imaging (ADAPT).

come the vulnerability of misdiagnosis (Despotović et al., 2015) and to speed the diagnosis process, the community has been using machine intelligence to help physicians diagnose AD diseases (Jo et al., 2019).

Considering the complex structure of brain magnetic resonance imaging (MRI), in recent years, Convolutional Neural Networks (CNNs) have been established with a dominant performance in the AD-related field (Salehi et al., 2020; Farooq et al., 2017), due to their effectiveness in extracting meaningful spatial hierarchical features from complex images. Many methods (Zhu et al., 2021; Wen et al., 2020) try to learn the characteristics of AD using CNN-based models. However, the original MRI is complex 3D data, with the proposed 3D model, the input of the 3D convolution operation introduces a third dimension, which greatly increases the burden on the computer. So they use a bag of patches selected from the skull-stripped brain region. These approaches disregard the global context information, which can have a substantial impact on accurately identifying lesions during inference (Wang et al., 2022). Moreover, CNNs are not well-suited for mining global long-dependent information due to their inherent focus on extracting local information (Luo et al., 2016; Dosovitskiy et al., 2020).

Transformers (Vaswani et al., 2017) have also been widely used in medical imaging because of their superior performances over CNNs. Such spatial relationships are crucial in 3D MRI images for Alzheimer’s diagnosis (Iaccarino et al., 2021), where understanding cross-sectional interdependencies is the key. However, transformer-based methods have yet to see widespread use in 3D medical image diagnosis. A primary reason is that due to a lack of inductive bias of locality, lower layers of ViT can not learn the local relations well, leading to the representation being unreliable (Zhu et al., 2023). Moreover, in 3D medical imaging, the scarcity of datasets, largely due to ethical considerations that restrict access (Setio et al., 2017; Simpson et al., 2019), costly annotations (Yu et al., 2019; Wang et al., 2023), class imbalance challenges (Yan et al., 2019), and the significant computational demands of processing high-dimensional data (Tajbakhsh et al., 2020), is a notable issue.

At the same time, these models typically treat all the dimensions in the same way. In contrast, when physicians read the MRI, they usually pay different attentions to different dimensions of the images, according to the atrophic patterns of the brain. This adaptive strategy of the physicians allows them to diagnose more efficiently and accurately.

Inspired by the above, we propose ADAPT, a pure transformer-based model that leverages the captured different features from each view dimension more smartly and efficiently. Our goal is to classify Alzheimer’s disease (AD) and normal states in 3D MRI images. The overall architecture of the proposed ADAPT model is shown in Fig 1. ADAPT factorizes 3D MRI images into three 2D sequences of slices along axial, coronal and sagittal dimensions. Then we combine multiple 2D slices as input and use a 2D separate transformer encoder model to classify. At the same time, we also build attention encoders across slices from the same dimension and the attention encoders across three dimensions. These encoders can help to efficiently combine the feature information better than just keep training using the slices altogether. Benefiting from the special encoder blocks, ADAPT can learn the AD pathology just using a few slices instead of inputting all 2D images, which can further reduce memory footprint. Our contribution is as follows:

- We proposed a new transformer-based architecture to solve the real-world AD diagnosis problem.
- We proposed a novel cross-attention mechanism and a novel guide patch embedding, which can gather the information between slices and sequences better.
- Considering the structure and difference between AD and normal MRI images, we designed the morphology augmentation methods to augment the data.
- We proposed an adaptive training strategy in order to guide the attention of our model, leading the model to

adaptively pay more attention to the more important dimension.

- Overall, we name our method ADAPT, which is evaluated as the state-of-the-art performance among all the baselines while occupying minimum memory.

2. Related Works

2.1. 3D Vision Transformer

The recent success of the transformer architecture in natural language processing (Vaswani et al., 2017) has garnered significant attention in the computer vision domain. The transformer has emerged as a substitute for traditional convolution operators, owing to its capacity to capture long-range dependencies. Vision Transformer (ViT) (Dosovitskiy et al., 2020) introduces transformer architecture into the computer vision field and starts a craze in combining transformers and images together. Many works have demonstrated remarkable achievements across various tasks, with several cutting-edge methods incorporating transformers for enhanced learning.

Some attention-based methods have been proposed for 3D image classification. COVID-ViT (Zhou et al., 2023a) uses 3D vision transformers to exploit CT chest information for the accurate classification of COVID. I3D (Carreira & Zisserman, 2017) proposes a new two-stream inflated 3D ConvNet to learn seamless spatio-temporal feature extractors from video, which can be used to do human action classification. At the same time, many existing works also deal with 3D object detection problems. Pointformer (Pan et al., 2021) captures and aggregates local and global features together to do both indoor and outdoor object detection. 3DERT (Misra et al., 2021) proposes an encoder-decoder module that can be applied directly on the point cloud for extracting feature information, and then predicting 3D bounding boxes. Also, image segmentation is a hot topic in the both computer vision and medical imaging fields. Swin UNETR (Hatamizadeh et al., 2021) projects multi-modal input data into a 1D sequence of embedding and uses it as input to an encoder composed of a hierarchical Swin Transformer (Liu et al., 2021).

Key Differences: These models are all using 3D architecture to deal with 3D input, which is inefficient in medical field due to the high value of medical images and limited dataset size. Unlike them, our 2D ADAPT utilizes different blocks to first extract features among different slices and dimensions, then use a cross-attention mechanism to combine these features together, which can better release the abilities of transformer architecture.

2.2. Deep Learning for Medical Image Analysis

With the success of deep learning models, extensive research interest has been devoted to deep learning for the development of novel medical image processing algorithms, resulting in remarkably successful deep learning-based models that effectively support disease detection and diagnosis in various medical imaging tasks (Chen et al., 2022). U-Net and its variants dominate medical image analysis, which is widely used in image segmentation. Attention U-Net (Oktay et al., 2018) incorporates attention gates into the U-Net architecture to learn important salient features and suppress irrelevant features.

For medical image classification, AG-CNN (Guan et al., 2018) uses the attention mechanism to identify discriminative regions from the global 2D image and fuse the global and local information together to better diagnose thorax disease from chest X-rays. MedicalNet (Chen et al., 2019) uses the resnet-based (He et al., 2016) model with transfer learning to solve the problem of lacking datasets. DomainKnowledge4AD (Zhou et al., 2023b) uses ResNet18 to extract high-dimensional features and proposes domain-knowledge encoding which can capture domain-invariant features and domain-specific features to help predict AD. M3T (Jang & Hwang, 2022) tries to leverage CNNs to capture the local features and use traditional transformer encoders for a long-range relationship in 3D MRI images.

Key Differences: These methods usually focus on CNN based model to extract and combine features, which has been outperformed by transformer-based models. M3T tries to concatenate transformer blocks after CNNs, however, they propose a much bigger model and treat all slices as the same which is inefficient. In our work, we use a pure transformer-based model with different kinds of encoders to do Alzheimer’s classification and have demonstrated ADAPT can outperform other deep learning models in both classification accuracy results and model size.

3. Methodology

3.1. ADAPT Architecture

Our model ADAPT builds upon the ViT architecture, extending it to model 3D images. Figure 2 shows the details. ADAPT mainly consists of 4 blocks:

- **Self-Attention Encoders (SAE)** across three views
- **Dimension-specific Self-Attention Encoders (DS-AE)**
- **Intra-dimension Cross-Attention Encoders (IntraCAE)**
- **Inter-dimension Cross-Attention Encoders (InterCAE)**

The design inspired from a real-world setting where physicians will pay different attentions to different views, according to the brain pattern. Thus, we design the encoders so that they not only can extract and fusion features from local

and global but also can give different weights to different views. To be specific, first, to better obtain the complete information of the 3D image, we cut each image along three views: sagittal view (along x-axis), coronal view (along y-axis), and axial view (along z-axis). We use n images from each view as the model input. Then similar to ViT, ADAPT also uses the image patch and patch embedding method to embed the 2D images into 3 sequences including $3 \times n$ slices with guide patch embedding layer \mathbf{x}_{guide} , then concatenates them together as the input to the transformer encoders (Eq. 1). The guide patch embedding aims to reshape the whole sequence into a sequence of flattened 2D patches that has the same shape as the sequence after the normal patch, which means the guide patch embedding has the input channel with the number $3 \times n$. Thus, we can use 3D models to extract the global information and add it to each special slice sequence. Because our model mainly focuses on 2D slice dimension, guide patch embedding can help to keep the relative position information of 3D brain.

$$\mathbf{S}_0 = [\underbrace{\mathbf{x}_{class}; \mathbf{x}_{p_1} + \mathbf{x}_{guide}; \cdots; \mathbf{x}_{p_n} + \mathbf{x}_{guide}}_{sagittal}; \underbrace{\cdots; \mathbf{x}_{p_{2n}} + \mathbf{x}_{guide}; \cdots; \mathbf{x}_{p_{3n}} + \mathbf{x}_{guide}}_{coronal}; \underbrace{\cdots; \mathbf{x}_{p_{3n}} + \mathbf{x}_{guide}}_{axial}] \quad (1)$$

$$\mathbf{S}_0 = \mathbf{S}_0 + \mathbf{E}_{pos} \quad \mathbf{E}_{pos} \in \mathbb{R}^{(3 \cdot n \cdot N + 1) \times D} \quad (2)$$

Second, the lower layer encoders learn the bias attention among multiple slices and multiple views. To be more specific, the shared Self-Attention Encoders (SAE) across three view dimensions are designed to learn not only the attention of the slice itself but also the relationship between all slices. The designed encoder can realize global information extraction for the first time. These encoders can also help to keep the relative position information of 3D MRI. These networks are Siamese networks (Guo et al., 2017) which share the same weights.

$$\mathbf{S}_0^s = [\mathbf{x}_{class}^s; \mathbf{x}_{p_s}] \quad s \in (1, 3 \cdot n) \quad (3)$$

$$\mathbf{S}_l^s = \text{SAE}(\mathbf{S}_{l-1}^s) \quad l = 1 \dots L_{SAE} \quad (4)$$

The Dimension-specific Self-Attention Encoders (DS-AE) also aim to learn the attention of the slice itself. However, compared with SAE, these encoders focus more on the relationship between the slices from the same dimension sequence. These encoders can better extract the local features from the same view dimension. This will fill the gap that transformers cannot capture the local features well however the local embeddings of different brain tissues (such as hippocampus and cortex) are really important in AD diagnosis. In the following equation, t means the three different views.

$$\mathbf{S}_l^{t,s} = \text{DSAE}_t(\mathbf{S}_{l-1}^{t,s}) \quad s \in (1, n), t \in (1, 3) \quad (5)$$

$$l = (L_{SAE} + 1) \dots (L_{SAE} + L_{DSAE})$$

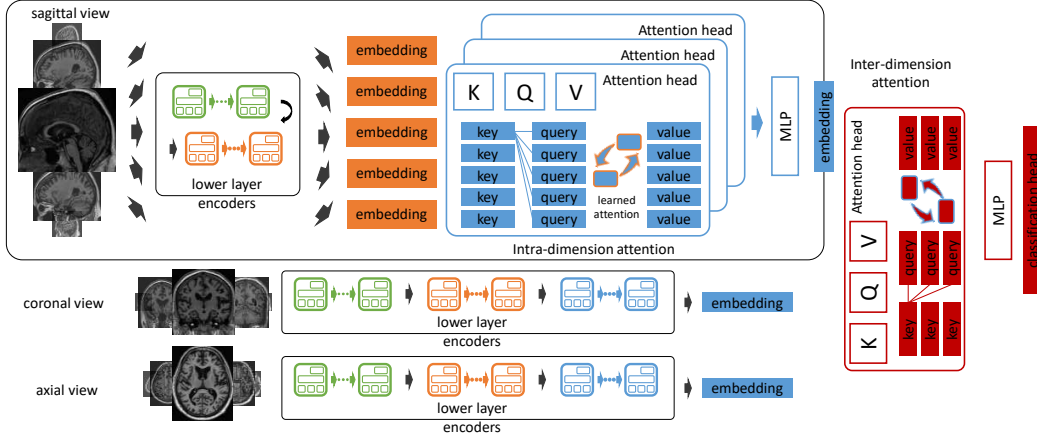


Figure 2. The detailed architecture for our ADAPT. ADAPT consists of four main components: **Self-Attention Encoders (SAE)** across three views, **Dimension-specific Self-Attention Encoders (DS-AE)**, **Intra-dimension Cross-Attention Encoders (IntraCAE)**, **Inter-dimension Cross-Attention Encoders (InterCAE)**. The figure shows more details in sagittal view for illustration purposes. In practice, the model will adaptively attend to different views.

We will fusion the local features from the same dimension first. So we design **Intra-dimension Cross-Attention Encoders (IntraCAE)**. Here ADAPT will apply cross embedding mechanism to the input embeddings. (Details are in section 3.2.) After the IntraCAE, the embeddings will gather the features from different slices of the same view sufficiently.

$$\begin{aligned} \mathbf{S}_l^{t,s} &= \text{IntraCAE}_t(\mathbf{S}_{l,t}^{t,s}) \quad s \in (1, n), t \in (1, 3) \\ l &= (L_{\text{SAE}} + L_{\text{DSAE}} + 1) \dots \\ &\quad (L_{\text{SAE}} + L_{\text{DSAE}} + L_{\text{IntraCAE}}) \end{aligned} \quad (6)$$

After combining the features between slices of the same dimension independently, the last **Inter-dimension Cross-Attention Encoders (InterCAE)** are proposed to learn the inter-dimension relationship among different sequences from different views. This is corresponding to the SAE layer and will gather the global features together. InterCAE will apply cross embedding mechanism again into the view-dependent embeddings.

$$\begin{aligned} \mathbf{S}_l^t &= \text{InterCAE}_t(\mathbf{S}_{l,t}^t) \quad t \in (1, 3) \\ l &= (L_{\text{SAE}} + L_{\text{DSAE}} + L_{\text{IntraCAE}} + 1) \dots \\ &\quad (L_{\text{SAE}} + L_{\text{DSAE}} + L_{\text{IntraCAE}} + L_{\text{InterCAE}}) \end{aligned} \quad (7)$$

Finally, the $[\text{class}]$ tokens of the output from three dimensions will be averaged and sent to Layer Norm and classification MLP head as Eq. ?? and Eq. ?? to get the final diagnosis result: AD or normal.

3.2. Fusion Attention Mechanism

The above architecture will allow us to learn the intricacies of AD pathologies along three different dimensions. However, the complicatedness of AD will require the model

to thoroughly integrate the information from these three dimensions. Thus, we propose a cross-attention mechanism, namely fusion attention. The fusion attention adds the embeddings together directly. However, different from simply adding them together one by one, it adds the embeddings representing the patches but not the tokens. Note that the $[\text{class}]$ token of each embedding has aggregated the information from one slice in previous encoders, so this operation will let the embeddings more focus on themselves when learning attention. At the same time, it can also extract the feature information from other slices or dimensions. The fusion attention applied to both IntraCAE and InterCAE, but here we use IntraCAE as an example:

$$\begin{aligned} \mathbf{S}_l^{t,s} &= \mathbf{x}_{\text{class}}^{t,s} \oplus (\mathbf{x}_{p_{(t-1) \cdot n+1}} + \dots + \mathbf{x}_{p_{t \cdot n}}) \\ \text{where } s &\in (1, n), t \in (1, 3) \end{aligned} \quad (8)$$

In a more formal way, the traditional attention mechanism is shown as Eq. 9. After fusing these two embeddings, the K matrix of the first embedding will consist of the K value corresponding to the $[\text{class}]$ token from the first embedding, and the K matrix corresponding to fusion embedding, similarly for Q matrix. After the matrix calculation, Eq. 11 fuses the information from two embeddings while keeping some unique information from the special $[\text{class}]$ token.

$$H = \text{softmax}\left(\frac{QK^T}{\sqrt{d_k}}\right)V \quad (9)$$

$$K_1 = [K_{\text{class}_1}, K_1 + K_2], Q_1 = [Q_{\text{class}_1}, Q_1 + Q_2] \quad (10)$$

$$Q_1 K_1^T = \begin{bmatrix} Q_{\text{class}_1} K_{\text{class}_1} & (Q_1 + Q_2) K_{\text{class}_1} \\ Q_{\text{class}_1} (K_1 + K_2) & (Q_1 + Q_2) (K_1 + K_2) \end{bmatrix} \quad (11)$$

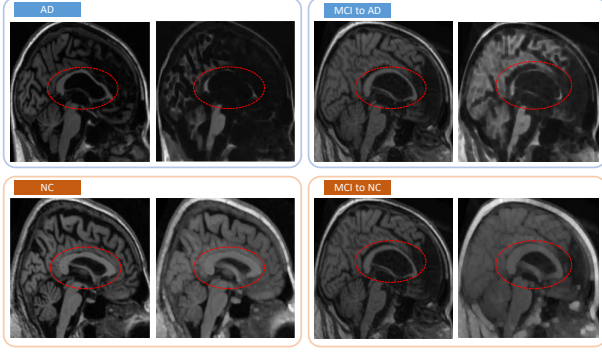


Figure 3. The visualization of Alzheimer's Disease (AD) image, Normal Control (NC) image and Mild Cognitive Impairment (MCI) image. The left is the raw image and the right is the augmented image. The cerebral ventricle (red circle) has a significant difference in size for AD and NC.

3.3. Morphology Augmentation

A key characteristic of the AD-plagued brain is that, as the disease progresses, an increasing amount of brain mass will suffer from atrophy. When this process is reflected in brain imaging, there will be empty "holes" of the brain if one has AD. Based on this, we propose a morphology augmentation, an augmentation method which help to expand and reduce the size of the atrophy, causing the improvement of the model. This augmentation is based on atrophy expansion and atrophy reduction shown in Eq. 12, 13. f is the input image, b_N is the atrophy expansion or atrophy reduction element, (x, y) and (s, t) are the coordinates in f and b_N respectively.

$$[f \ominus b_N](x, y) = \min_{(s, t) \in b_N} \{f(x + s, y + t) - b_N(s, t)\} \quad (12)$$

$$[f \oplus b_N](x, y) = \max_{(s, t) \in b_N} \{f(x - s, y - t) + b_N(s, t)\} \quad (13)$$

We apply atrophy expansion augmentation to AD images and MCI images and label the resultant images as AD; on the other hand, we apply atrophy reduction augmentation to Normal Control (NC) images and MCI images and label the resultant images as NC, where MCI is the prodromal stage of AD. The visualization of morphology augmentation is shown in Fig. 3.

3.4. Adaptive Training Strategy

To further investigate the potential of ADAPT, we propose an attention score based training strategy in order to allow our model to extract more features from the more important dimension with limited size of inputs. We calculate the attention score of each dimension after the final inter-dimension cross attention encoder layer according to Eq. 14. Because our $[class]$ token is dimension specific, so we just

calculate the attention score of the $[class]$ token as the representation of the special dimension. This strategy allows our network to adaptively choose the slice number of each dimension while updating itself.

$$H_{dim} = softmax(\frac{Q_{class_{dim}} K^T}{\sqrt{d_k}}) V \quad (14)$$

Algorithm 1 ADAPT Training Strategy

Input: 3D MRI Training set T , initial slice number list ψ , model ADAPT Θ , total slice number n_{total}

Output: Updated model Θ , final list ψ

```

1: while Training do
2:   Sample 2D data  $\delta$  with  $T$  and  $\psi$ 
3:    $TRAIN(\Theta, \delta)$ 
4:   Calculate score using Eq. 14 for three dimensions
5:   Calculate cross-entropy loss and update  $\Theta$ 
6:   if  $p$  then
7:     Update  $\psi$  according to Eq 16, 15.
8:   else
9:      $INITIALIZE(\psi)$ 
10:  end if
11: end while
    
```

We then adaptively update the slice number of each dimension based on normalized attention scores using Eq. 15, 16, where n is the total slice number and ψ is the slice number list. Here we also constrain the selection pool to make sure the model will attend across multiple attentions. The full training strategy is shown in algorithm 1. To avoid the model will stick with certain view dimension after the first choice, we also allow the model to change the attention with certain probabilities p .

$$n_{dim} = round(\frac{H_{dim}}{\sum_{r \in \psi} r} * n_{total}) \quad (15)$$

$$n_{dim} = \begin{cases} n_{min}, n_{dim} \geq n_{min} \\ n_{max}, n_{dim} \leq n_{max} \end{cases} \quad (16)$$

4. Experiments

4.1. Experimental Dataset

To verify the effectiveness of our ADAPT, we use the dataset from the Alzheimer's Disease Neuroimaging Initiative (ADNI) for the training process. This dataset consists of MRI images of T1-weighted magnetic resonance imaging subjects. There are a total of 3,891 3D MRI images in the dataset, including 1,216 normal cases (NC), 1,110 AD cases and 1,565 MCI cases. During the training, 878 normal images, 884 AD images and 1565 MCI images were split into the training set, with 72 normal images and 81 AD

Model name	Model size (#params)	GFLOPs	ADNI		AIBL	MIRIAD	OASIS
			val acc.	test acc.	test acc.	test acc.	test acc.
MedicalNet-10 (Chen et al., 2019)	17,723,458	225.7	0.827	0.843	0.856	0.847	0.793
MedicalNet-18 (Chen et al., 2019)	36,527,938	492.6	0.756	0.793	0.820	0.800	0.809
MedicalNet-34 (Chen et al., 2019)	66,837,570	910.8	0.571	0.669	0.847	0.782	0.585
MedicalNet-50 (Chen et al., 2019)	59,626,818	666.8	0.588	0.471	0.303	0.706	0.317
MedicalNet-101 (Chen et al., 2019)	98,672,962	1181.1	0.558	0.425	0.320	0.656	0.291
MedicalNet-152 (Chen et al., 2019)	130,831,682	1604.8	0.564	0.381	0.175	0.662	0.239
3D ResNet-34 (He et al., 2016)	63,470,658	341.1	0.506	0.618	0.779	0.453	0.745
3D ResNet-50 (He et al., 2016)	46,159,170	256.9	0.519	0.618	0.776	0.657	0.720
3D ResNet-101 (He et al., 2016)	85,205,314	391.1	0.569	0.526	0.601	0.426	0.433
3D DenseNet-121 (Huang et al., 2017)	11,244,674	260.5	0.609	0.675	0.816	0.408	0.772
3D DenseNet-201 (Huang et al., 2017)	25,334,658	286.8	0.564	0.612	0.672	0.553	0.671
Knowledge4D (Zhou et al., 2023b)	33,162,880	633.9	0.603	0.728	0.845	0.658	0.784
I3d (Carreira & Zisserman, 2017)	12,247,332	191.0	0.513	0.629	0.674	0.448	0.607
FCNlinksCNN (Qiu et al., 2020)	310,488,372	375.6	0.423	0.614	0.708	0.370	0.691
COVID-ViT (Gao et al., 2021)	78,177,282	448.6	0.506	0.573	0.644	0.662	0.715
Uni4Eye (Cai et al., 2022)	340,324,866	78.4	0.622	0.646	0.697	0.647	0.688
ADAPT	9,695,490	46.3	0.904	0.924	0.910	0.903	0.817

Table 1. Comparison of accuracy various 3D CNN-based and transformer-based models on multi-institutional Alzheimer’s disease dataset.

images as a validation set, together with 266 normal images and 145 AD images as a testing set.

At the same time, to evaluate the performance of our ADAPT and other deep learning baseline models, we also consider other datasets as test sets. We mainly acquire them from three other institutions with the ADNI test dataset: Australian Imaging, Biomarker and Lifestyle Flagship Study of Ageing (AIBL), Minimal Interval Resonance Imaging in Alzheimer’s Disease (MIRIAD), and The Open Access Series of Imaging Studies (OASIS). The AIBL dataset contains a total of 413 images with 363 NC and 50 AD after dropping all MCI cases. The MIRIAD dataset contains a total of 523 cases which consist of 177 NC and 346 AD cases. The OASIS dataset contains a total of 2157 cases which consist of 1692 NC and 465 AD cases. Each of the images for any dataset is a 3D grayscale image.

4.2. Implementation Details

We implement consistent data pre-processing techniques to normalize and standardize MRI images sourced from a multi-institutional database. We first do data augmentation in the following steps. we have followed closely the recommended protocol from the medical community (Wen et al., 2020) to process the data. Firstly, we do bias field correction with N4ITK method (Tustison et al., 2010). Next, we register each image to the MNI space (Fonov et al., 2009; 2011) with the ICBM 2009c nonlinear symmetric template by performing a affine registration using the SyN algorithm (Avants et al., 2014) from ANTs (Avants

et al., 2008). At the same time, the registered images were further cropped to remove the background to improve the computational efficiency. These operations result in 1 mm isotropic voxels for each image. Intensity rescaling, which was performed based on the minimum and maximum values, denoted as MinMax, was also set to be optional to study its influence on the classification results. Finally, the deep QC system (Fonov et al., 2018) is performed to check the quality of the linearly registered data. The software outputs a probability indicating how accurate the registration is. We excluded the scans with a probability lower than 0.5. Overall, the registration process we perform on the data maps different sets of images into a single coordinate system to prepare the data for our later usage.

We also use the Torchio library (Pérez-García et al., 2021) in the training set. At the same time, we resize all the MRI images with Scipy library (Virtanen et al., 2020) into $224 \times 224 \times 224$ to better fit the input of our ADAPT. Finally, we employed the zero-mean unit-variance method to normalize the intensity of all voxels within the images.

For the training dataset, we apply morphology augmentation to the same MCI data, classify the MCI into NC after doing atrophy reduction augmentation, and classify it into AD after doing atrophy expansion augmentation. In this way, each MCI is used twice, significantly enlarging the dataset. At the same time, we also do morphology augmentation to AD and NC images randomly, with a probability of 0.5.

After preprocessing the 3D MRI images, we cut them into 2D slices along sagittal, coronal and axial views. Then we

choose 16 slices in each view as the initial data and concatenate them into a sequence. We choose equidistant slices on each view and embed them into patch embedding similar to ViT. Here we choose the embed layer from (Touvron et al., 2022). Then we use a total of 6 standard transformer attention layers, and 1 layer for each of the first two encoders, 2 layers for each of the last two encoders, with 4 heads. For the adaptive training strategy, we set the probability p as 0.8. At last, because we have three $[class]$ tokens, each representing a special view dimension, we use a classification MLP head, with input feature number 3×256 and output feature number 2, aiming to figure out whether the image is from a disease or not.

We implemented ADAPT using a Pytorch library (Paszke et al., 2019). ADAPT was trained using an AdamW optimizer with a learning rate of 0.00005. All other parameters are default. At the same time, we also took the advantage of cosine learning rate from (Loshchilov & Hutter, 2016). We treat this as a binary classification task, so we use cross-entropy loss (Zhang & Sabuncu, 2018). The training process used 2 80G NVIDIA A800 GPUs. Due to the memory capacity, we use 6 batches on each GPU, meaning a total batch size of 12.

4.3. Evaluation Between Baselines

Our ADAPT was compared with various baseline models, including 3D CNN-based models: 3D DenseNet (121, 201) (Huang et al., 2017), 3D ResNet (34, 50, 101) (He et al., 2016) because they have been widely used for AD classification (Korolev et al., 2017; Ruiz et al., 2020; Yang et al., 2018; Zhang et al., 2021). We also add other baselines to show the capability of our ADAPT, including: MedicalNet (Chen et al., 2019), I3D (Carreira & Zisserman, 2017), FCNlinksCNN (Qiu et al., 2020) and Knowledge4D (Zhou et al., 2023b). There are various versions of MedicalNet, each of which is based on a basic Resnet (He et al., 2016) model, such that MedicalNet-10 is based on Resnet-10 respectively. We also compare our method with 3D transformer-based models: COVID-ViT (Gao et al., 2021), Uni4Eye (Cai et al., 2022).

In the experiment, we chose a total of 48 slices as input, meaning 16 equidistant slices on each view as initial. Because we found that the central part of the 3D images would be more important and consist of more useful information, we applied the **important sampling** method in our slice-picking stage. To be more specific, for a $224 \times 224 \times 224$ image, we pick equidistant slices from 52nd to 172nd on each view.

The quantitative performance is presented in Table 1. We chose the model with the best validation accuracy on ADNI and then tested it on various Alzheimer’s disease datasets. We also recorded the total parameters and GFLOPs of each

Layer Number	ADNI		AIBL		MIRIAD		OASIS	
	Val acc.	Test acc.	Test acc.	Test acc.	Test acc.	Test acc.	Test acc.	Test acc.
1+1+1+1	0.713	0.776	0.800	0.685	0.793			
2+2+1+1	0.770	0.811	0.863	0.903	0.716			
2+2+2+2	0.881	0.911	0.897	0.669	0.800			
3+3+3+3	0.917	0.895	0.907	0.723	0.806			
Ours (1+1+2+2)	0.904	0.924	0.910	0.903	0.817			

Table 2. Comparison of accuracy between ADAPT and three variants ablating with different numbers of transformer layers in each encoder in the four datasets.

Cross-Attention Mechanism	ADNI		AIBL		MIRIAD		OASIS	
	Val acc.	Test acc.	Test acc.	Test acc.	Test acc.	Test acc.	Test acc.	Test acc.
No Cross-Attention	0.719	0.627	0.810	0.710	0.675			
Class Token Cross-Attention	0.878	0.848	0.864	0.709	0.606			
Easy Concat Cross-Attention	0.917	0.783	0.723	0.806	0.681			
Ours (Fusion Attention)	0.904	0.924	0.910	0.903	0.817			

Table 3. Comparison of accuracy between ADAPT and three variants ablating different cross attention mechanisms in the four datasets.

model. Overall, ADAPT achieves the best performance on i.i.d testing scenario (ADNI) as well as all out-of-domain testing scenarios (AIBL, MIRIAD and OASIS). We believe these results show that ADAPT is not only superior in Alzheimer’s diagnosis in i.i.d setting, but also fairly robust when the testing data is collected from different facilities. At the same time, our model has the least parameters and GLOPs, demonstrating the success of our novel method in attacking the AD diagnosing task using 2D based model.

The best performance is achieved when ADAPT chooses 10 slices from sagittal view, and 19 slices from the coronal and axial view respectively. As compared with table 4, we found the interesting facts that coronal and axial view may contain more differential relationships about cortex and ventricle of AD and NC, which can help the model learn the special attention features accurately.

4.4. Ablation Study

To evaluate how effective each block is, we compared our ADAPT with other variants, changing one setting each time. We first changed the transformer attention layers of each

Models	ADNI		AIBL		MIRIAD		OASIS	
	Val acc.	Test acc.	Test acc.	Test acc.	Test acc.	Test acc.	Test acc.	Test acc.
w/o Morphology Augmentation	0.604	0.738	0.889	0.828	0.792			
w/o Adaptive Training	0.788	0.855	0.883	0.902	0.807			
w/o Guide Eembedding	0.750	0.800	0.863	0.869	0.813			
w/o Torchio	0.678	0.755	0.825	0.664	0.783			
w/o Pretrained Weights	0.731	0.738	0.877	0.746	0.800			
w/o Important Sampling	0.713	0.712	0.757	0.767	0.787			
ADAPT	0.904	0.924	0.910	0.903	0.817			

Table 4. Comparison of accuracy between ADAPT and five variants ablating different training augmentation settings in the four datasets.

encoder. We investigate how the number of layers will affect our ADAPT performance. The results are shown in Table 2, there are four numbers in each variant, each one corresponding to an encoder block. Such as 1+1+2+2 meaning that the shared self-attention encoders, dimension-specific self-attention encoders, intra-dimension cross-attention encoders and inter-dimension cross-attention encoders have 1, 1, 2, 2 transformer attention layer respectively. The result shows that ADAPT outperforms all the variants on test accuracy in three out of four datasets (ADNI, AIBL, MIRIAD) while using small enough memory.

Table 3 shows how different cross-attention mechanisms will affect the final result. The first variant: No Cross-Attention, meaning that we didn’t apply any cross-attention mechanism in the last two encoder blocks. Class Token Cross-Attention is a variant of Eq. 10. It adds the $[class]$ token embedding up but not the embedding behind the $[class]$ token. For the easy concat cross-attention mechanism, it simply concatenates the embeddings from different slices and view dimensions into a whole large embedding. Our proposed Fusion Attention achieves more than 7% improvements to the ADNI test result while demonstrating superiority on other testing datasets, verifying that fusion attention cannot only fuse the information while keeping the unique information in each embedding.

Table 4 shows other variables in our settings. We delete one important setting in each variant to see the results. ADAPT outperforms all variant models in all four datasets by 4.9%, 2.1%, 0.1% and 1.0%, respectively. The results show the great capability of different settings in augmenting the model learning ability to classify 3D MRI.

4.5. Visualization Result

We visualize the activated area our model focusing on based on the transformer attention map. Figure 4 shows a NC-related attention map in 3D MRI images from ADNI dataset in sagittal, coronal and axial views. Because ADAPT has 4 special encoders, we visualize the attention result after each encoder.

We found that for NC and AD result, the attention mostly focused on some special brain tissues, such as hippocampus, cortex, ventricle and frontal lobe. Disruption of the frontal lobes and its associated networks are a common consequence of neurodegenerative disorders (Sawyer et al., 2017), as well as the hippocampus is most notably damaged by AD (Xu et al., 2021). Based on these understandings of Alzheimer’s pathology (Frisoni et al., 2010), ADAPT successfully captured the AD-related part because with the procedure of Alzheimer’s, the hippocampus and cortex begin to atrophy, and the ventricle begins to expand, which can serve as an evidence of morphology augmentation and confirm the reliability of our proposed ADAPT.

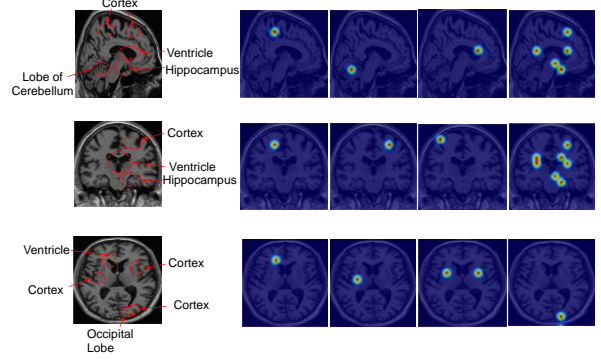


Figure 4. Attention map for Normal Control result. Each line corresponds to one view dimension: sagittal, coronal and axial.

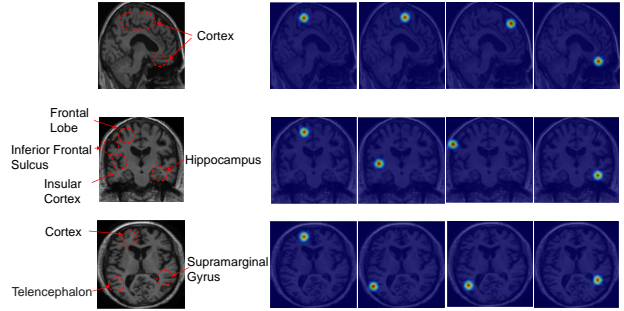


Figure 5. Attention map for Alzheimer’s Disease result. Each line corresponds to one view dimension: sagittal, coronal and axial.

5. Conclusions

We proposed a 3D medical image classification model, called ADAPT, that uses various 2D transformer encoder blocks for Alzheimer’s disease diagnosis. The proposed method uses shared self-attention encoders across different view dimensions, dimension-specific self-attention encoders, intra-dimension cross-attention encoders, and inter-dimension cross-attention encoders to extract and combine information from high-dimensional 3D MRI images, with novel techniques such as fusion attention mechanism and morphology augmentation. With different encoders, our adaptive training strategy can allow physicians to pay more attention to different dimensions of MRI images. The experiments show that ADAPT can achieve outstanding performance while utilizing the least memory compared to various 3D image classification networks in multi-institutional test datasets. The visualization results show that ADAPT can successfully focus on AD-related regions of 3D MRI images, guiding accurate and efficient clinical research on Alzheimer’s Disease.

Impact Statements

This paper presents work whose goal is to advance the field of Machine Learning and Alzheimer’s Diagnosis. We hope our work can provide insights for medical doctors and help them diagnose AD in a convenient way. We suggest that our model should be used under human supervision to ensure a perfect result. There are many other potential societal consequences of our work, none which we feel must be specifically highlighted here.

References

- Avants, B. B., Epstein, C. L., Grossman, M., and Gee, J. C. Symmetric diffeomorphic image registration with cross-correlation: evaluating automated labeling of elderly and neurodegenerative brain. *Medical image analysis*, 12(1): 26–41, 2008.
- Avants, B. B., Tustison, N. J., Stauffer, M., Song, G., Wu, B., and Gee, J. C. The insight toolkit image registration framework. *Frontiers in neuroinformatics*, 8:44, 2014.
- Cai, Z., Lin, L., He, H., and Tang, X. Uni4eye: Unified 2d and 3d self-supervised pre-training via masked image modeling transformer for ophthalmic image classification. In *International Conference on Medical Image Computing and Computer-Assisted Intervention*, pp. 88–98. Springer, 2022.
- Carreira, J. and Zisserman, A. Quo vadis, action recognition? a new model and the kinetics dataset. In *proceedings of the IEEE Conference on Computer Vision and Pattern Recognition*, pp. 6299–6308, 2017.
- Chen, S., Ma, K., and Zheng, Y. Med3d: Transfer learning for 3d medical image analysis. *arXiv preprint arXiv:1904.00625*, 2019.
- Chen, X., Wang, X., Zhang, K., Fung, K.-M., Thai, T. C., Moore, K., Mannel, R. S., Liu, H., Zheng, B., and Qiu, Y. Recent advances and clinical applications of deep learning in medical image analysis. *Medical Image Analysis*, 79:102444, 2022.
- Despotović, I., Goossens, B., Philips, W., et al. Mri segmentation of the human brain: challenges, methods, and applications. *Computational and mathematical methods in medicine*, 2015, 2015.
- Dosovitskiy, A., Beyer, L., Kolesnikov, A., Weissenborn, D., Zhai, X., Unterthiner, T., Dehghani, M., Minderer, M., Heigold, G., Gelly, S., et al. An image is worth 16x16 words: Transformers for image recognition at scale. *arXiv preprint arXiv:2010.11929*, 2020.
- Farooq, A., Anwar, S., Awais, M., and Rehman, S. A deep cnn based multi-class classification of alzheimer’s disease using mri. In *2017 IEEE International Conference on Imaging systems and techniques (IST)*, pp. 1–6. IEEE, 2017.
- Fonov, V., Evans, A. C., Botteron, K., Almli, C. R., McKinsty, R. C., Collins, D. L., Group, B. D. C., et al. Unbiased average age-appropriate atlases for pediatric studies. *Neuroimage*, 54(1):313–327, 2011.
- Fonov, V. S., Evans, A. C., McKinsty, R. C., Almli, C. R., and Collins, D. Unbiased nonlinear average age-appropriate brain templates from birth to adulthood. *NeuroImage*, 47:S102, 2009.
- Fonov, V. S., Dadar, M., Group, P.-A. R., and Collins, D. L. Deep learning of quality control for stereotaxic registration of human brain mri. *bioRxiv*, pp. 303487, 2018.
- Frisoni, G. B., Fox, N. C., Jack Jr, C. R., Scheltens, P., and Thompson, P. M. The clinical use of structural mri in alzheimer disease. *Nature Reviews Neurology*, 6(2): 67–77, 2010.
- Gao, X., Qian, Y., and Gao, A. Covid-vit: Classification of covid-19 from ct chest images based on vision transformer models. *arXiv preprint arXiv:2107.01682*, 2021.
- Guan, Q., Huang, Y., Zhong, Z., Zheng, Z., Zheng, L., and Yang, Y. Diagnose like a radiologist: Attention guided convolutional neural network for thorax disease classification. *arXiv preprint arXiv:1801.09927*, 2018.
- Guo, Q., Feng, W., Zhou, C., Huang, R., Wan, L., and Wang, S. Learning dynamic siamese network for visual object tracking. In *Proceedings of the IEEE international conference on computer vision*, pp. 1763–1771, 2017.
- Hatamizadeh, A., Nath, V., Tang, Y., Yang, D., Roth, H. R., and Xu, D. Swin unetr: Swin transformers for semantic segmentation of brain tumors in mri images. In *International MICCAI Brainlesion Workshop*, pp. 272–284. Springer, 2021.
- He, K., Zhang, X., Ren, S., and Sun, J. Deep residual learning for image recognition. In *Proceedings of the IEEE conference on computer vision and pattern recognition*, pp. 770–778, 2016.
- Huang, G., Liu, Z., Van Der Maaten, L., and Weinberger, K. Q. Densely connected convolutional networks. In *Proceedings of the IEEE conference on computer vision and pattern recognition*, pp. 4700–4708, 2017.
- Iaccarino, L., La Joie, R., Edwards, L., Strom, A., Schonhaut, D. R., Ossenkoppele, R., Pham, J., Mellinger, T., Janabi, M., Baker, S. L., et al. Spatial relationships between molecular pathology and neurodegeneration in the alzheimer’s disease continuum. *Cerebral Cortex*, 31(1): 1–14, 2021.

- Jang, J. and Hwang, D. M3t: three-dimensional medical image classifier using multi-plane and multi-slice transformer. In *Proceedings of the IEEE/CVF conference on computer vision and pattern recognition*, pp. 20718–20729, 2022.
- Jo, T., Nho, K., and Saykin, A. J. Deep learning in alzheimer's disease: diagnostic classification and prognostic prediction using neuroimaging data. *Frontiers in aging neuroscience*, 11:220, 2019.
- Korolev, S., Safiullin, A., Belyaev, M., and Dodonova, Y. Residual and plain convolutional neural networks for 3d brain mri classification. In *2017 IEEE 14th international symposium on biomedical imaging (ISBI 2017)*, pp. 835–838. IEEE, 2017.
- Liu, Z., Lin, Y., Cao, Y., Hu, H., Wei, Y., Zhang, Z., Lin, S., and Guo, B. Swin transformer: Hierarchical vision transformer using shifted windows. In *Proceedings of the IEEE/CVF international conference on computer vision*, pp. 10012–10022, 2021.
- Loshchilov, I. and Hutter, F. Sgdr: Stochastic gradient descent with warm restarts. *arXiv preprint arXiv:1608.03983*, 2016.
- Luo, W., Li, Y., Urtasun, R., and Zemel, R. Understanding the effective receptive field in deep convolutional neural networks. *Advances in neural information processing systems*, 29, 2016.
- Misra, I., Girdhar, R., and Joulin, A. An end-to-end transformer model for 3d object detection. In *Proceedings of the IEEE/CVF International Conference on Computer Vision*, pp. 2906–2917, 2021.
- Oktay, O., Schlemper, J., Folgoc, L. L., Lee, M., Heinrich, M., Misawa, K., Mori, K., McDonagh, S., Hammerla, N. Y., Kainz, B., et al. Attention u-net: Learning where to look for the pancreas. *arXiv preprint arXiv:1804.03999*, 2018.
- Pan, X., Xia, Z., Song, S., Li, L. E., and Huang, G. 3d object detection with pointformer. In *Proceedings of the IEEE/CVF Conference on Computer Vision and Pattern Recognition*, pp. 7463–7472, 2021.
- Paszke, A., Gross, S., Massa, F., Lerer, A., Bradbury, J., Chanan, G., Killeen, T., Lin, Z., Gimelshein, N., Antiga, L., et al. Pytorch: An imperative style, high-performance deep learning library. *Advances in neural information processing systems*, 32, 2019.
- Pérez-García, F., Sparks, R., and Ourselin, S. Torchio: a python library for efficient loading, preprocessing, augmentation and patch-based sampling of medical images in deep learning. *Computer Methods and Programs in Biomedicine*, 208:106236, 2021.
- Qiu, S., Joshi, P. S., Miller, M. I., Xue, C., Zhou, X., Karjadi, C., Chang, G. H., Joshi, A. S., Dwyer, B., Zhu, S., et al. Development and validation of an interpretable deep learning framework for alzheimer's disease classification. *Brain*, 143(6):1920–1933, 2020.
- Ruiz, J., Mahmud, M., Modasshir, M., Shamim Kaiser, M., and Alzheimer's Disease Neuroimaging Initiative, f. t. 3d densenet ensemble in 4-way classification of alzheimer's disease. In *Brain Informatics: 13th International Conference, BI 2020, Padua, Italy, September 19, 2020, Proceedings 13*, pp. 85–96. Springer, 2020.
- Salehi, A. W., Baglat, P., Sharma, B. B., Gupta, G., and Upadhyay, A. A cnn model: earlier diagnosis and classification of alzheimer disease using mri. In *2020 International Conference on Smart Electronics and Communication (ICOSEC)*, pp. 156–161. IEEE, 2020.
- Sawyer, R. P., Rodriguez-Porcel, F., Hagen, M., Shatz, R., and Espay, A. J. Diagnosing the frontal variant of alzheimer's disease: a clinician's yellow brick road. *Journal of clinical movement disorders*, 4:1–9, 2017.
- Setio, A. A. A., Traverso, A., De Bel, T., Berens, M. S., Van Den Bogaard, C., Cerello, P., Chen, H., Dou, Q., Fantacci, M. E., Geurts, B., et al. Validation, comparison, and combination of algorithms for automatic detection of pulmonary nodules in computed tomography images: the luna16 challenge. *Medical image analysis*, 42:1–13, 2017.
- Simpson, A. L., Antonelli, M., Bakas, S., Bilello, M., Farahani, K., Van Ginneken, B., Kopp-Schneider, A., Landman, B. A., Litjens, G., Menze, B., et al. A large annotated medical image dataset for the development and evaluation of segmentation algorithms. *arXiv preprint arXiv:1902.09063*, 2019.
- Tajbakhsh, N., Jeyaseelan, L., Li, Q., Chiang, J. N., Wu, Z., and Ding, X. Embracing imperfect datasets: A review of deep learning solutions for medical image segmentation. *Medical Image Analysis*, 63:101693, 2020.
- Touvron, H., Cord, M., El-Nouby, A., Verbeek, J., and Jégou, H. Three things everyone should know about vision transformers. In *European Conference on Computer Vision*, pp. 497–515. Springer, 2022.
- Tustison, N. J., Avants, B. B., Cook, P. A., Zheng, Y., Egan, A., Yushkevich, P. A., and Gee, J. C. N4itk: improved n3 bias correction. *IEEE transactions on medical imaging*, 29(6):1310–1320, 2010.
- Vaswani, A., Shazeer, N., Parmar, N., Uszkoreit, J., Jones, L., Gomez, A. N., Kaiser, Ł., and Polosukhin, I. Attention is all you need. *Advances in neural information processing systems*, 30, 2017.

- Virtanen, P., Gommers, R., Oliphant, T. E., Haberland, M., Reddy, T., Cournapeau, D., Burovski, E., Peterson, P., Weckesser, W., Bright, J., et al. Scipy 1.0: fundamental algorithms for scientific computing in python. *Nature methods*, 17(3):261–272, 2020.
- Wang, H., Lin, L., Hu, H., Chen, Q., Li, Y., Iwamoto, Y., Han, X.-H., Chen, Y.-W., and Tong, R. Super-resolution based patch-free 3d medical image segmentation with self-supervised guidance. *arXiv preprint arXiv:2210.14645*, 2022.
- Wang, Y., Tu, Z., Xiang, Y., Zhou, S., Chen, X., Li, B., and Zhang, T. Rapid image labeling via neuro-symbolic learning. *arXiv preprint arXiv:2306.10490*, 2023.
- Wen, J., Thibeau-Sutre, E., Diaz-Melo, M., Samper-González, J., Routier, A., Bottani, S., Dormont, D., Durrleman, S., Burgos, N., Colliot, O., et al. Convolutional neural networks for classification of alzheimer’s disease: Overview and reproducible evaluation. *Medical image analysis*, 63:101694, 2020.
- Xu, F., Ono, M., Ito, T., Uchiumi, O., Wang, F., Zhang, Y., Sun, P., Zhang, Q., Yamaki, S., Yamamoto, R., et al. Remodeling of projections from ventral hippocampus to prefrontal cortex in alzheimer’s mice. *Journal of Comparative Neurology*, 529(7):1486–1498, 2021.
- Yan, K., Peng, Y., Sandfort, V., Bagheri, M., Lu, Z., and Summers, R. M. Holistic and comprehensive annotation of clinically significant findings on diverse ct images: learning from radiology reports and label ontology. In *Proceedings of the IEEE/CVF Conference on Computer Vision and Pattern Recognition*, pp. 8523–8532, 2019.
- Yang, C., Rangarajan, A., and Ranka, S. Visual explanations from deep 3d convolutional neural networks for alzheimer’s disease classification. In *AMIA annual symposium proceedings*, volume 2018, pp. 1571. American Medical Informatics Association, 2018.
- Yu, L., Wang, S., Li, X., Fu, C.-W., and Heng, P.-A. Uncertainty-aware self-ensembling model for semi-supervised 3d left atrium segmentation. In *Medical Image Computing and Computer Assisted Intervention–MICCAI 2019: 22nd International Conference, Shenzhen, China, October 13–17, 2019, Proceedings, Part II* 22, pp. 605–613. Springer, 2019.
- Zhang, J., Zheng, B., Gao, A., Feng, X., Liang, D., and Long, X. A 3d densely connected convolution neural network with connection-wise attention mechanism for alzheimer’s disease classification. *Magnetic Resonance Imaging*, 78:119–126, 2021.
- Zhang, Z. and Sabuncu, M. Generalized cross entropy loss for training deep neural networks with noisy labels. *Advances in neural information processing systems*, 31, 2018.
- Zhou, X., Zhou, W., Fu, X., Hu, Y., and Liu, J. Mdv: introducing mobile three-dimensional convolution to a vision transformer for hyperspectral image classification. *International Journal of Digital Earth*, 16(1):1469–1490, 2023a.
- Zhou, Y., Li, Y., Zhou, F., Liu, Y., and Tu, L. Learning with domain-knowledge for generalizable prediction of alzheimer’s disease from multi-site structural mri. In *International Conference on Medical Image Computing and Computer-Assisted Intervention*, pp. 452–461. Springer, 2023b.
- Zhu, H., Chen, B., and Yang, C. Understanding why vit trains badly on small datasets: An intuitive perspective. *arXiv preprint arXiv:2302.03751*, 2023.
- Zhu, W., Sun, L., Huang, J., Han, L., and Zhang, D. Dual attention multi-instance deep learning for alzheimer’s disease diagnosis with structural mri. *IEEE Transactions on Medical Imaging*, 40(9):2354–2366, 2021.